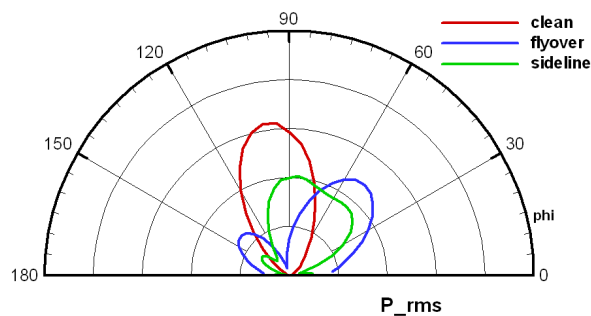




Executive summary

Analytical method for the computation of the noise from a pusher propeller



Problem area

One of the possible concepts for future small aircraft is a configuration equipped with a single-rotating pusher propeller. As the concern about the environmental impact by aviation is still growing, design tools for such an aircraft have to include methods for the evaluation of emissions and noise.

The noise of a pusher propeller is significantly different from that of a tractor propeller, because of the aerodynamic interference between the inflow, which is disturbed by engine exhausts and wakes from upstream airframe parts, and the propeller blades. The purpose of the work described in this paper is to develop a fast and easy-to-use computational method for the noise of a pusher propeller in a prescribed inflow.

Description of work

An existing lifting-line method has been extended to incorporate a non-uniform inflow into the propeller. The method was applied to a test case from the EU-project CESAR (Cost-Effective Small Aircraft).

Results and conclusions

Results from the method have been compared to results from a fully computational approach (CFD/CAA). The agreement between both sets of results is fair, and the preliminary conclusion, pending availability of test data, is that the method satisfies its purpose.

Report no.

NLR-TP-2010-580

Author(s)

H.H. Brouwer

Report classification

UNCLASSIFIED

Date

July 2011

Knowledge area(s)

Aëro-akoestisch en experimenteel aërodynamisch onderzoek

Descriptor(s)

Propeller Noise

Applicability

The computational method described in this report is ready to use for the computation of the noise from a pusher propeller. As input it requires the propeller geometry, operational conditions, and a description of the steady, non-uniform inflow in the propeller disc. As such it can be used for an assessment of the noise impact from a pusher propeller configuration, in an early stage of the aircraft design, or in the case of introduction of such aircraft at a specific airport.



NLR-TP-2010-580

Analytical method for the computation of the noise from a pusher propeller

H.H. Brouwer


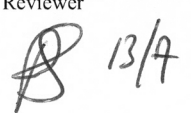

This report is based on a presentation held at the 16th AIAA/CEAS Aeroacoustics Conference, Stockholm, Sweden, 7-9 June 2010.

The contents of this report may be cited on condition that full credit is given to NLR and the authors.

This publication has been refereed by the Advisory Committee AEROSPACE VEHICLES.

Customer	European Commission
Contract number	AIP5-CT-2006-030888
Owner	NLR
Division NLR	Aerospace Vehicles
Distribution	Unlimited
Classification of title	Unclassified
	July 2011

Approved by:

Author 	Reviewer 	Managing department 
---	---	--

Contents

Nomenclature	4
I. Introduction	5
II. Mathematical model	5
III. Definition of test case	8
IV. Far-field results	10
V. Near-field results	11
VI. Variation of blade number	13
VII. Conclusions	13
Acknowledgments	13
References	13

Analytical method for the computation of the noise from a pusher propeller

Harry H. Brouwer¹

National Aerospace Laboratory NLR, 1006 BM Amsterdam, The Netherlands

The noise of a pusher propeller is significantly different from that of a tractor propeller, because of the aerodynamic interference between the inflow, which is disturbed by engine exhausts and wakes from upstream airframe parts, and the propeller blades. In this paper a fast and easy-to-use method is presented for the computation of the noise of a pusher propeller. An analytical description is derived for the interaction noise caused by a steady, non-uniform inflow into a propeller. The method is based on a Fourier-decomposition of the inflow, and a lifting-line description of the unsteady forces on the propeller blades. This analytical description has been implemented in a computer program and applied to a test case. Comparison of the results to results from a fully computational approach yields a reasonable agreement in a qualitative sense, which suggests that the method at least captures the physics of the problem. A limited parameter study is presented.

Nomenclature

B	= blade number
c	= local blade chord
c_0	= speed of sound
c_l	= lift coefficient
k	= wave number
L	= lift per unit span
M	= main flow Mach number
p	= acoustic pressure
r	= radial co-ordinate
r_h	= hub radius
S	= Sears function
t	= time
\vec{U}_∞	= helical relative flow velocity
\vec{v}	= velocity perturbation
\vec{v}_i	= time-averaged induced velocity
\vec{V}_∞	= main flow velocity
x	= axial co-ordinate
β	= $\sqrt{1 - U_\infty^2 / c_0^2}$
γ	= radial wavenumber
θ	= azimuthal angle
κ	= $\sqrt{(\omega / c_0)^2 - (\gamma\beta)^2}$
λ	= wavelength
ρ_0	= density of air
ρ	= secondary radial co-ordinate
ω	= angular frequency
Ω	= propeller angular speed

¹ Senior Scientist, Department of Helicopters and Aeroacoustics, P.O. Box 90502.

I. Introduction

ONE of the possible concepts for future small aircraft is a configuration equipped with a single-rotating pusher propeller. As the concern about the environmental impact by aviation is still growing, design tools for such an aircraft have to include methods for the evaluation of emissions and noise.

The noise of a pusher propeller is significantly different from that of a tractor propeller, because of the aerodynamic interference between the inflow, which is disturbed by engine exhausts and wakes from upstream airframe parts, and the propeller blades. The purpose of the work described in this paper is to develop a fast and easy-to-use computational method for the noise of a pusher propeller in a prescribed inflow.

Computation methods for propeller noise exist in many varieties. High-fidelity models are based on a detailed numerical simulation, using Computational Fluid Dynamics (CFD), of the unsteady flow about the entire propulsion system, or even about the whole aircraft. The acoustic radiation in such cases is usually described by using a Kirchhoff surface, or by application of the Ffowcs-Williams/Hawkings equations^{1,2}. Such a method offers the advantage that the interaction of the flow and the propeller are adequately taken into account, including the perturbations in the flow caused by other parts of the aircraft. For the application of such methods there is no fundamental difference between tractor and pusher propellers. A drawback of CFD-based methods is that for each new configuration, even for a change in blade angle, a new computational grid has to be generated. A second drawback is the computation time required; to obtain the acoustic data, time-accurate computations are required, covering a long time span to find the low-frequency components. An accurate description of the high-frequency components requires small time steps and fine computation grids.

A much simpler method is the lifting-line approach, in which each propeller blade is regarded as a spanwise distribution of aerodynamic forces. These forces can be found by application of the method of Matched Asymptotic Expansions, linking the local lift at each radial station and the induced flow about the blade. The analytic description of such a model and its application to isolated tractor propellers in a uniform flow, was published in Ref. 3. The validity of this model is restricted to classical propellers, with blades of high aspect ratio, in a uniform flow. On the other hand, the set of input data for this method is very limited, and computation time is negligible. A lifting-line method is therefore very suitable for parameter studies and preliminary design optimizations.

In the present paper it is presented how an existing lifting-line method is extended to incorporate a non-uniform inflow into the propeller.

In section II an analytical description is derived for the noise caused by a steady, non-uniform inflow into a propeller. The method is based on a Fourier-decomposition of the inflow, and a lifting-line description of the unsteady forces on the propeller blades. The additional acoustic pressure is regarded as a perturbation that is linear in the flow perturbation. In section III a test case is defined, and the results for this case are presented in sections IV (far-field) and V (near-field). Results for a different blade number are presented in section VI, as an example of a parameter study. Conclusions are given in section VII.

II. Mathematical model

The analysis starts with a single-rotating propeller, which rotates about the x -axis with angular speed Ω , in a uniform main flow \vec{V}_∞ in the positive x -direction. The main flow is perturbed by a parallel velocity field, which is specified in the propeller plane ($x = 0$):

$$\vec{v}(y, z) = v(y, z)\vec{e}_x \quad (1)$$

In the sequel we will work with the Fourier components of v in circumferential direction:

$$v(r, \theta) = \sum_{n=-\infty}^{\infty} \hat{v}_n(r) e^{in\theta} \quad (2)$$

where $y = r \cos\theta$, $z = r \sin\theta$.

The coordinate systems used are depicted in Fig. 1.

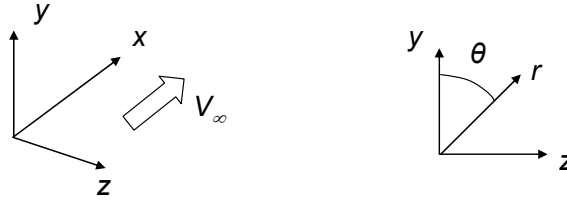


Figure 1. Cartesian and cylindrical coordinate system

The flow perturbation causes a fluctuation in the angle of attack at a local blade section that is given in first order in v/U_∞ by (Fig. 2):

$$\delta\psi = \psi - \psi_0 = \arctan\left(\frac{\Omega r}{V_\infty + v}\right) - \arctan\left(\frac{\Omega r}{V_\infty}\right) \approx \frac{-v\Omega r}{U_\infty^2} \quad (3)$$

where $U_\infty = \sqrt{V_\infty^2 + (\Omega r)^2}$.

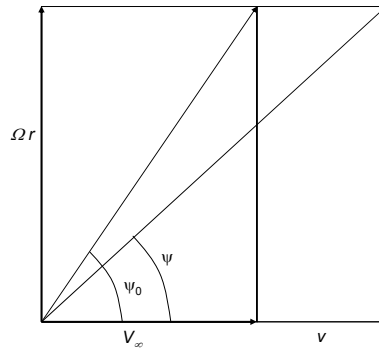


Figure 2. Relative flow directions

In a quasi-steady approach, and within the thin-airfoil approximation, the fluctuation of the lift is given by:

$$\delta L = \frac{1}{2} \rho_0 U_\infty^2 c \delta c_l = \frac{-\pi \rho c |\Omega| r}{\beta} v \quad (4)$$

with ρ_0 the density of air, c the local blade chord, $\beta = \sqrt{1 - U_\infty^2 / c_0^2}$, with c_0 the speed of sound, and c_l the lift coefficient. In order to be able to make some numerical estimates, a typical take-off case is specified:

Propeller tip radius:	1 m
Rotational speed:	2000 RPM
Flight speed:	80 m/s
Local blade chord (0.7 radius):	0.2 m
Altitude:	sea level

The helical speed at 0.7 radius is 167 m/s ($M \approx 0.5$). A gust impinging on the blade section at $0.7R$, R being the tip radius, will thus take 1 ms to pass from leading to trailing edge, which is 1/30 of the revolution time. It is therefore questionable if the flow disturbance caused by a wake can be treated as quasi-steady. To account for the

finite response time of the lift to the flow perturbation, we incorporate the incompressible Sears function, which is frequency-dependent (see e.g. Ref. 4). We now find for the n -th component of the Fourier-transformed fluctuation of the lift:

$$\delta \hat{L}_n = \frac{-\pi \rho_0 c |\Omega| r}{\beta} S(k_n) \hat{v}_n \quad (5)$$

where

$$S(k) = \frac{1}{\frac{\pi}{2} k (H_0^{(2)}(k) - i H_1^{(2)}(k))} \quad (6)$$

and $k_n = n |\Omega| c / 2U_\infty$. Incompressibility can be assumed if the upstream travel time of a pressure disturbance from the trailing edge to the leading edge is shorter than a period of oscillation:

$$\frac{c}{c_0 - U_\infty} < \frac{2\pi}{n |\Omega|} \quad (7)$$

In our example this condition is fulfilled for $n < 26$, which seems to be quite sufficient. Within the lifting line approximation³, the additional acoustic pressure δp , caused by the lift fluctuation $\delta \vec{L}$, satisfies:

$$\left[\left(\frac{1}{c_0} \frac{\partial}{\partial t} + M \frac{\partial}{\partial x} \right)^2 - \nabla^2 \right] \delta p = \sum_{j=1}^B \nabla \cdot \frac{1}{r} \delta \vec{L} \delta(x) \delta(\theta - \Omega t - 2\pi j / B) \quad (8)$$

The magnitude of the lift fluctuation is given by eq. (5). With respect to its direction we make the approximation that it is perpendicular to the local relative main flow, taking into account the time-averaged induced velocity, see figure 3. The latter is computed with the aerodynamic lifting-line method³.

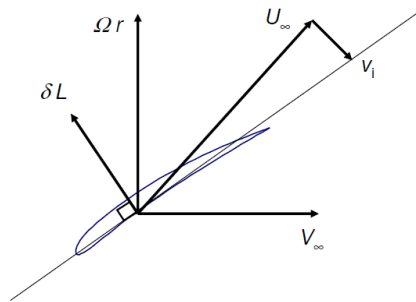


Figure 3. Direction of lift fluctuation δL ($\delta L > 0$).

To solve eq. (8) we use the Green's function from Ref. 5:

$$G(r, \theta, x, t | \rho, \chi, \xi, \tau) = \frac{1}{(2\pi)^2} \sum_{m=-\infty}^{\infty} e^{im(\theta-\chi)} \int_{-\infty}^{\infty} e^{i\omega(t-\tau)} \int_0^{\infty} \frac{\gamma J_m(\gamma r) J_m(\gamma \rho)}{2i\kappa(\gamma, \omega)} e^{-i(x-\xi)k_\xi} d\gamma d\omega \quad (9)$$

with:

$$\kappa^2(\gamma, \omega) = (\omega / c_0)^2 - (\gamma\beta)^2, \text{Im } \kappa < 0,$$

$$k_\xi = -[M\omega / c_0 - \text{sgn}(x - \xi)\kappa(\gamma, \omega)] / \beta^2$$

For the solution of eq. (8) we find:

$$\delta p = \frac{B}{4\pi} \sum_{n=-\infty}^{\infty} \sum_{m=-\infty}^{\infty} \int_0^R \int_{r_h}^R \frac{\gamma J_{nB+m}(\gamma r) J_{nB+m}(\gamma \rho)}{\kappa(\gamma, -nB\Omega)} e^{-ik_x x} e^{inB(\theta - \Omega t) + im\theta} \times$$

$$\left[k_x \vec{i}_x - \frac{nB+m}{\rho} \vec{i}_\theta \right] \cdot \delta \vec{L}_m(\rho) d\rho d\gamma \quad (10)$$

with $k_x = [MnB\Omega / c_0 + \text{sgn}(x)\kappa(\gamma, -nB\Omega)] / \beta^2$, and r_h the hub radius.

If we define d and $\tilde{\varphi}$ by:

$$r = d \sin \tilde{\varphi}, \quad x = -\sqrt{1 - M^2} d \cos \tilde{\varphi} \quad (11)$$

a far-field expression can be derived⁶. For $d \rightarrow \infty$ we find:

$$\delta p = \frac{iB}{4\pi d \beta} \sum_{n=-\infty}^{\infty} \sum_{m=-\infty}^{\infty} e^{inB(\theta - \Omega t) + im\theta} e^{-i \text{sgn}(nB\Omega)[(nB+m)\pi/2 - \gamma_s d (M \cos \tilde{\varphi} + 1)]}$$

$$\int_{r_h}^R J_{nB+m}(\gamma_s \rho \sin \tilde{\varphi}) \left[k_x \vec{i}_x - \frac{nB+m}{\rho} \vec{i}_\theta \right] \cdot \delta \vec{L}_m(\rho) d\rho \quad (12)$$

with $k_x = nB\Omega[M + \cos \tilde{\varphi}] / (c_0 \beta^2)$ and $\gamma_s = |nB\Omega| / (c_0 \beta)$. Along the axis, for which $\sin \tilde{\varphi} \rightarrow 0$, the Bessel function in the integrand vanishes, except for $nB + m = 0$. This means that the directivity pattern of each circumferential mode has zeros at the propeller axis, unless $nB + m = 0$, which is the '0' mode, i.e. the mode that does not depend on the angle θ .

The chain of computations is as follows:

- Computation of the aerodynamic performance of the propeller. This is done for the simplest, uninstalled configuration, i.e. the isolated propeller in a steady, uniform flow, parallel to the axis. This computation, also done within the lifting-line approximation³, yields the induced angle of attack and the steady lift at each radial station.
- The acoustic pressure is computed for the uninstalled propeller, at the specified observer positions.
- The aircraft angle of incidence is incorporated, by computing the additional noise caused by the vertical component of the relative main flow. The resulting total noise levels will be referred to hereafter as that of the 'clean' propeller.
- The axial perturbation velocity is Fourier-transformed in circumferential direction for each radial station, see eq. (2).
- The additional noise caused by the inflow perturbations is computed according to eqs. (5) and (10), and added to the noise of the clean propeller.

III. Definition of test case

The computational method of section II is implemented in a computer program, which is applied to an available test case. This test case is taken from the EU funded CESAR project (Cost-Effective Small Aircraft⁷), which is representative of an industrially relevant pusher-propeller aircraft. It is derived from the Piaggio P180 Avanti, equipped with two 5-bladed pusher propellers. Each engine has two circular exhaust exits.

Computations are made for the propeller at starboard, which is rotating clock-wise when looking in the direction of the flow (positive x-direction). Hence the sign of \mathcal{Q} is positive.

Computations have been made for the following configuration:

Altitude:	3000 ft
Flight Mach nr.:	0.235
RPM:	2000

The numerically computed inflow data, i.e. the flow perturbation velocity data, were provided by DLR¹. These flow data have been computed with an unsteady RANS method (URANS), incorporating viscous effects and propeller motion. Also the engine inlet flow and exhaust jet have been modelled by applying the appropriate boundary conditions. As the flow solution represents time-dependent flow perturbations, the data had to be averaged in time for the present application. The time-averaged axial flow velocity just upstream of the propeller plane is shown in Figure 4.

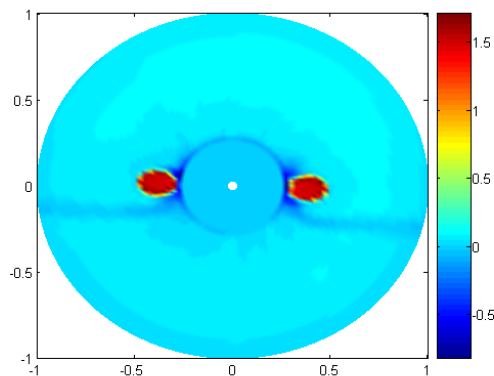


Figure 4. Perturbation velocity upstream of the propeller plane. Dimensions scaled on propeller radius, velocity on V_∞ .

For $r < 0.25R$ no data are available, and the perturbation is set to zero. The exhaust flow is clearly visible as two hot spots near the horizontal. Also the velocity deficit in the wake of the wing is visible.

IV. Far-field results

In Fig. 5 results are shown for the Fourier coefficients of the flow perturbation, for the two most relevant radial stations.

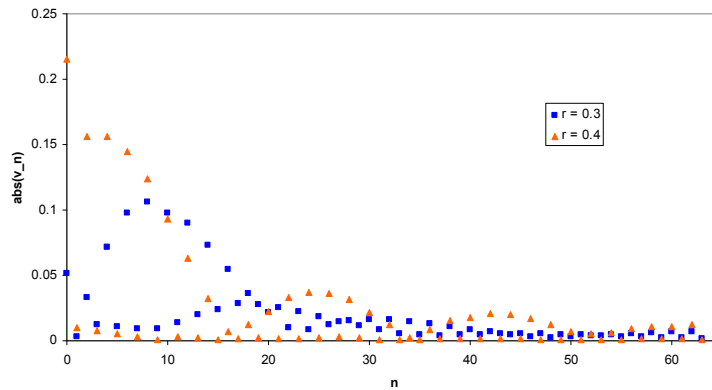


Figure 5. Absolute values of the Fourier coefficients of the flow perturbation shown in Fig. 4. Radii are relative to tip radius, velocities to V_∞ .

Note that because of the symmetry in the exhaust jets, the even components are much larger than the odd components. The far field results are obtained by computing the noise levels at a sideline at $10R$, which are then scaled to a constant radius of $10R$. The noise is computed for two observer lines, corresponding to the choice made in reference 1, i.e. flyover, $\theta = 180^\circ$, and sideline, $\theta = 270^\circ$. In Fig. 6 directivity plots of the *rms* of the acoustic pressure, BPF and $2 \times$ BPF tone, are shown. The polar angle $\varphi = 0^\circ$ corresponds to the flight direction.

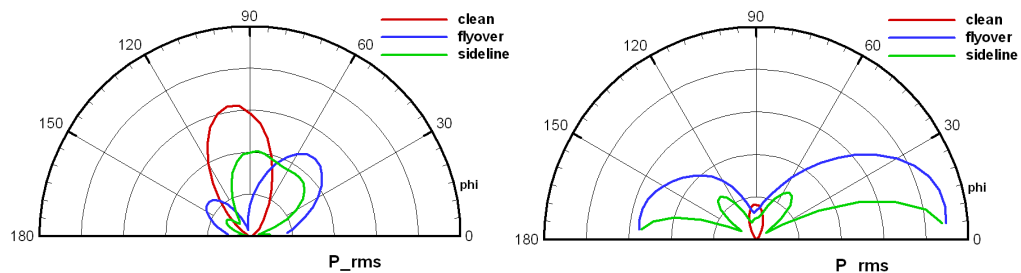


Figure 6. Far-field p_{rms} , BPF (left) and $2 \times$ BPF (right) tone.

It is remarkable that in the region near the propeller plane, the ‘installed’ noise level is lower than that of the clean propeller, in both the flyover and sideline direction. This means that at these angles the additional noise caused by the interaction with the inflow is largely cancelling the noise of the clean propeller. For the $2 \times$ BPF tone the difference between the clean and installed configuration is much larger, especially for the radiation near the propeller axis. This can be explained by the fact that the directivity on the axis is only non-zero for $nB + m = 0$, for the m -th Fourier component of the velocity perturbation. As these components are much larger for even values of m than for odd values, the ‘0’ mode is hardly excited for $n = 1$, but it is significantly excited for $n = 2$ (remember that $B = 5$).

V. Near-field results

No measured data are available for the present test case and only a comparison with results computed with other methods is possible. In this section near-field results are presented for two observer lines at a distance of $r = 4R$, again corresponding to flyover, $\theta = 180^\circ$, and sideline, $\theta = 270^\circ$, see Fig. 7. These are the same positions as analyzed in Ref. 1, where results are presented that are obtained with a CFD/CAA method. Results from the latter method, as used here for comparison, were computed by application of the Ffowcs-Williams/Hawkings equations to the unsteady pressures on the airframe and propeller blade surfaces^{1,2}. These unsteady pressure data were part of the URANS solution, as briefly described in section III.

The levels of the BPF at the flyover observer line are compared in Fig. 8. The results from the present method are labeled ‘NLR’, those from Ref. 1 are labeled ‘DLR’.

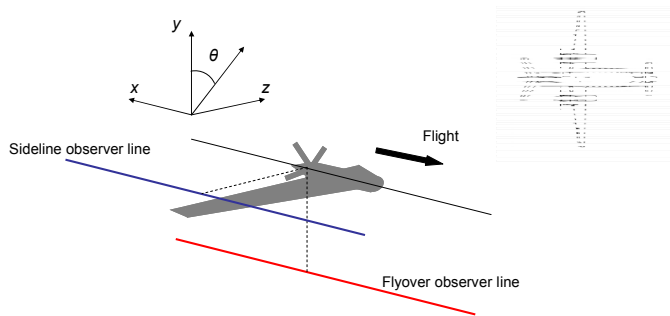


Figure 7. Sketch of starboard wing/nacelle and observer lines.

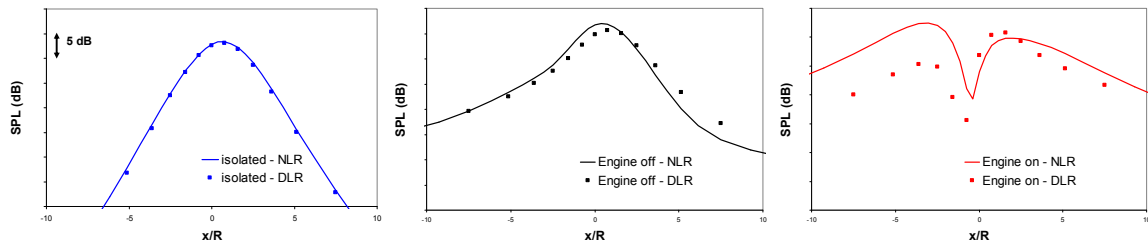


Figure 8. Comparison of results from the present method to those of Ref. 1. BPF, flyover.

The ‘isolated’ case corresponds to the isolated propeller in a uniform axial main flow, the ‘engine off’ case to the installed propeller, but without the exhaust flow, i.e. only the wake of the wing is incorporated, the ‘engine on’ case corresponds to the installed propeller in the complete perturbation flow as depicted in Figure 4. For the isolated propeller the agreement is excellent, for the other two cases the general shape of the curve is the same, but the difference in the absolute level exceeds 5 dB at some locations.

For the higher harmonics the differences become larger, see Fig. 9. It is expected that the results from the lifting-line approximation will become less reliable, as this is in fact an approximation for high values of λ/c , with λ the acoustic wavelength, and c the local blade chord, a criterion that is violated for the higher harmonics.

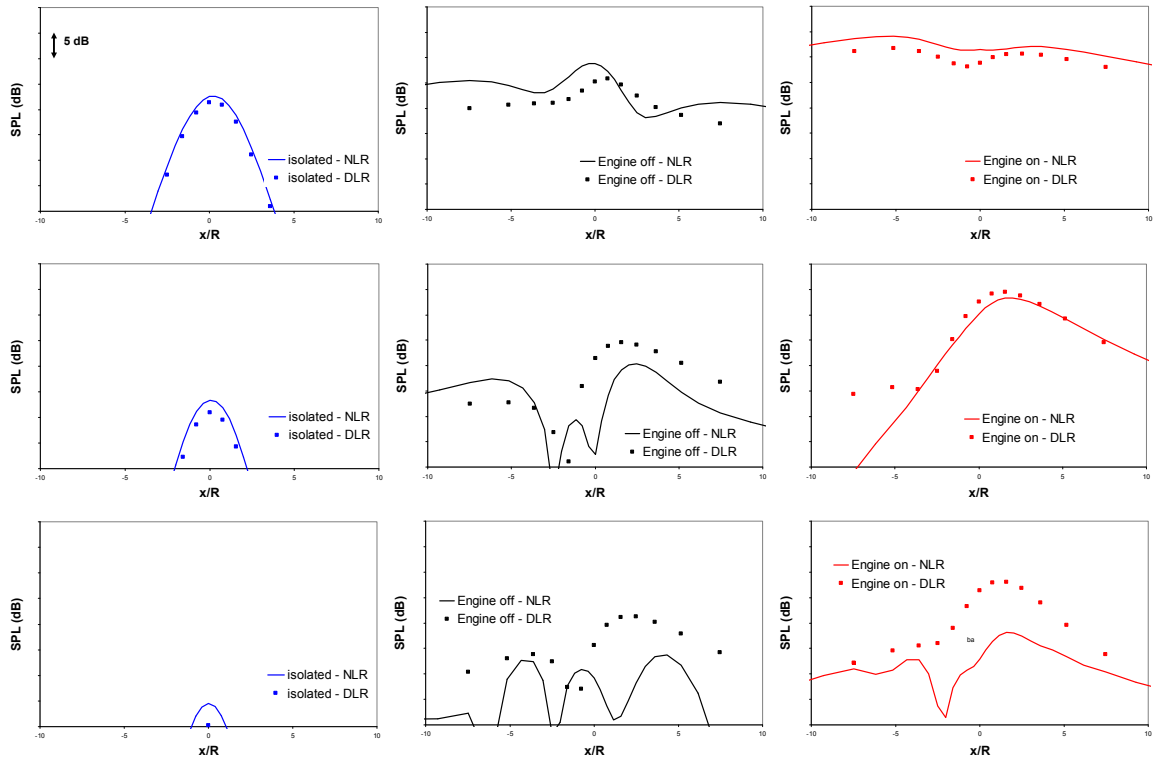


Figure 9. Comparison of results from the present method to those of Ref. 1. 2x BPF, 3x BPF, and 4x BPF, flyover.

In Fig. 10 the total A-weighted noise levels are plotted, for both the flyover and sideline observer lines.

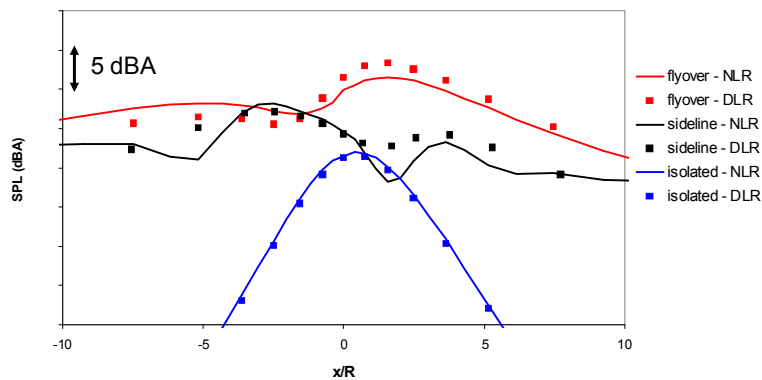


Figure 10. Total A-weighted noise levels.

Although the results from both methods do not match perfectly, it seems that the present method does capture the physics of the acoustics of a propeller in a nonuniform inflow. The main two differences between the noise levels of an isolated propeller and those of an installed propeller are:

- The noise levels of the installed propeller are considerably higher; near the propeller plane differences are found higher than 10 dBA.
- The directivity is completely different; while the sound field of an isolated propeller is concentrated near the propeller plane, an installed pusher propeller also radiates in the rear and forward arc.

VI. Variation of blade number

In this section results for the noise of an installed 6-bladed propeller are presented. To this end we take the same blades as in the previous section. Two options are investigated, with the same thrust as the case studied above:

- ⇒ The same rotational speed, 2000 RPM. In order to maintain the same thrust, the blade angle is reduced.
- ⇒ A reduced rotational speed, i.e. 1700 RPM instead of 2000 RPM, which corresponds to the choice made in Ref. 8. The blade angle is now increased to maintain the same thrust.

The inflow perturbation is not changed for these cases. Because of the simplicity of the lifting-line method, at least with respect to the ease of use, the assessment of these additional cases only requires a few changes in the input data, and running the aerodynamic and acoustic programs, with a turn-around time of a few seconds. The results for both flyover and sideline noise levels are shown in Figure 11.

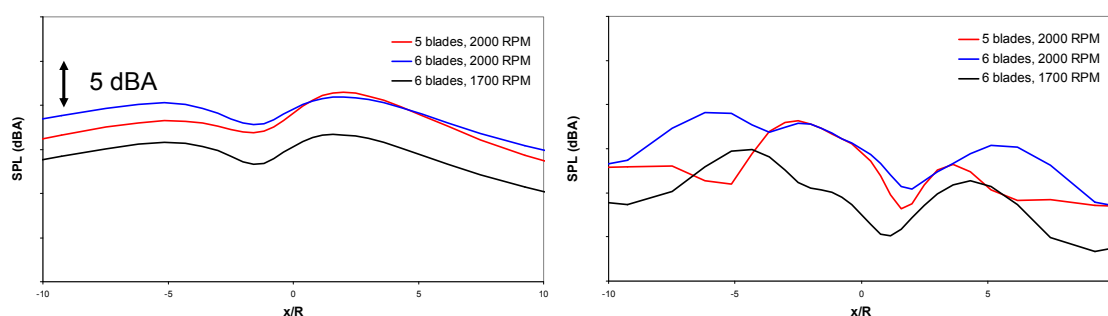


Figure 11. Flyover (left) and sideline (right) noise levels of 3 installed propeller configurations: 5-bladed / 2000 RPM, 6-bladed / 2000 RPM, 6-bladed / 1700 RPM.

In contrast to a tractor propeller, increasing the blade number as such does not reduce the noise level. Only when also the RPM is reduced, a lower noise level is obtained. This can be explained by the fact that the interaction BPF tone is not very much excited for an odd number of blades in a symmetric flow perturbation, while it is efficiently excited for an even number of blades.

VII. Conclusions

The purpose of the work described in this report was to develop a fast and easy-to-use computational method for the noise of a pusher propeller in a prescribed inflow.

An analytical description has been derived for the interaction noise caused by a steady, non-uniform inflow into a propeller. The method is based on a Fourier-decomposition of the inflow, and a lifting-line description of the unsteady forces on the propeller blades. This analytical description has been implemented in a computer program, which was applied to test cases available in the CESAR project. No measured data are available from these test cases, and absolute accuracy of the results can not be assessed yet. However, comparison of the results to results from a fully computational approach (CFD/CAA) yields a reasonable agreement, which suggests that the method at least captures the physics of the problem.

The analytical nature of the method enables a detailed breakdown of the computed noise levels, which shows that the levels, and the directivity, depend strongly on the symmetry properties of the non-uniform inflow, and the blade number of the propeller.

The computation method has been applied to a configuration with an increased blade number. It appears that, unlike for the case of a propeller in a uniform flow, increasing the blade number as such does not reduce the noise level. Only when also the RPM is reduced, a lower noise level is obtained.

Acknowledgments

This work was carried out in the framework of the CESAR project (Cost-Effective Small Aircraft), co-funded by the European Commission. The author thanks Jianping Yin and Arne Stuermer of DLR for sharing their data.

References

- ¹Yin, J., Stuermer, A., and Aversano, M., "Coupled uRANS and FW-H Analysis of Installed Pusher Propeller Aircraft Configurations", *15th AIAA/CEAS Aeroacoustics Conference*, Miami, FL, AIAA Paper 2009-3332, 2009.



- ²Pagano, A., Barbarino, M., Casalino, D., and Federico, L., "Tonal and Broadband Noise Calculations for Aeroacoustic Optimization of Propeller Blades in a Pusher Configuration", *15th AIAA/CEAS Aeroacoustics Conference*, Miami, FL, AIAA Paper 2009-3138, 2009.
- ³Brouwer, H.H., "On the use of matched asymptotic expansions in propeller aerodynamics and acoustics", *J. Fluid Mech.*, Vol.242, pp.117-143, 1992.
- ⁴Howe, M.S., *Acoustics of fluid-structure interactions*, Cambridge University Press, 1998.
- ⁵Schulten, J.B.H.M., "A spectral method for the computation of propeller acoustics", *AIAA 11th Aeroacoustics Conference*, Palo Alto, CA, AIAA Paper 87-2674, 1987.
- ⁶Brouwer, H.H., "A lifting line model for propeller noise", *AIAA 12th Aeroacoustics Conference*, San Antonio, TX, AIAA Paper 89-1079, 1989.
- ⁷CESAR, <http://www.cesar-project.eu>, web page, 2009.
- ⁸Ianniello, S., Di Mascio, A., Salvatore, F., Sollo, A., Aversano, M., Gennaretti, M., "Evaluation of noise excess for pushing propeller aircraft by CFD aeroacoustic calculation", *10th AIAA/CEAS Aeroacoustics Conference*, Manchester, UK, AIAA Paper 2004-3006, 2004.